STRUCTURAL CHARACTERIZATION OF WELDED AL6060-T5 ALLOY JOINTS BY FRICTION STIR SPOT WELDING UNDER CORROSION ATACK

CARACTERIZAÇÃO ESTRUTURAL DE JUNTAS DE LIGA AL6060-T5 SOLDADAS POR PONTOS DE FRICÇÃO SOB ATAQUE DA CORROSÃO

CARACTERIZACIÓN ESTRUCTURAL DE UNIONES DE ALEACIÓN AL6060-T5 SOLDADAS POR PUNTO DE FRICCIÓN BAJO ATAQUE DE CORROSIÓN

Ana Cláudia Costa de Oliveira[1]
Hortencia Noronha dos Santos[2]
Paulo Paiva Oliveira Leite Dyer[3]
Silvelene Alessandra Silva[4]
Kahl Dick Zilnyk[5]
Maria Margareth da Silva[6]
Getúlio de Vasconcelos[7]
Tonilson de Souza Rosendo[8]

Abstract: Al6060-T5 alloys are widely used in the aerospace, shipbuilding and automotive industries. Nevertheless, the conventional welding process could be weakening its resistance to corrosion. Thus, Friction Stir Spot Welding (FSSW) becomes an alternative to reduce the thermally affected zone (HAZ) at the joints. Although, persist a lack of studies, on current literature, about these welding properties; as welds its corrosion resistance. With this in mind, this present paper evaluated an Al6060-T5 alloy plates welds after periods of 336, 672 and 1008 hours into 3.5% NaCl electrolyte immersion. Where, for each period, the plates were evaluated in terms of open circuit potentials (OCP), micro hardness Vickers, elemental composition and its corrosion severity. The results shown a percentage increasing of oxygen rate (3 to 4%); identifying corrosive activity in the mixing zone. Likewise, electrochemical tests shown a greater susceptibility to corrosion at weld nearing centre regions; due to Mg and Si precipitates presence. Even so, all immersion times samples presented a mild corrosive severity.

Key words: Aluminium Alloy Al6060-T5; corrosion resistance; friction stir welding; FSSW; immersion corrosion.

---

[1] Professora de Materiais da Universidade Federal de Lavras - UFLA. Doutora em Engenharia Aeroespacial INPE. E-mail: anaclaudia.oliveira@ufla.br.
[2] Mestrado em Engenharia Mecânica pela Universidade Federal do Pampa - Unipampa. E-mail: hortencia.noronha@gmail.com.
[3] Doutorado em Ciências pelo Instituto Tecnológico de Aeronáutica - ITA, São José dos Campos, São Paulo, Brasil. E-mail: paulo_dyer@yahoo.com.
[4] Pós-doutorado em Laser Cladding pelo Instituto de Estudos Avançados - IEAv, São José dos Campos, São Paulo. E-mail: lenisoni@uol.com.br.
[5] Professor de Materiais e Processos de Fabricação do Instituto Tecnológico de Aeronáutica - ITA. Doutor em Engenharia de Materiais pela Escola de Engenharia de Lorena da Universidade de São Paulo E-mail: zilny@ita.br.
[6] Professora de Materiais do Instituto Tecnológico de Aeronáutica - ITA. Doutora Engenharia Aeronáutica e Mecânica pelo Instituto Tecnológico de Aeronáutica. E-mail: meg@ita.br.
[7] Pesquisador Instituto de Estudos Avançados – IEAv, e doutorado em Ciências, na área de Tecnologia Nuclear- Materiais pelo Instituto de Pesquisas Energéticas e Nucleares. E-mail: getulio@ieav.cta.br.
[8] Resumo do autor: Professor da Universidade Federal do Pampa - Unipampa. E-mail: tonilsonrosendo@unipampa.edu.br.

Resumo: As ligas Al6060-T5 são amplamente utilizadas na indústria aeroespacial, naval e automobilista. Contudo, a soldagem convencional pode enfraquecer sua resistência a corrosão. Assim, a soldagem Friction Stir Spot Welding (FSSW) se torna uma alternativa para reduzir a zona termicamente afetada (ZTA) na junta. Neste horizonte, este artigo avaliou soldas de chapas de Al6060-T5 em períodos de 336, 672 e 1008 horas de imersão em NaCl 3,5%. Para cada período, as chapas foram avaliadas quanto ao potencial de circuito fechado (PCA), dureza Vickers, composição elementar e severidade corrosiva. Os resultados mostraram um aumento percentual de Oxigênio (3 a 4%); identificando atividade corrosiva na zona de mistura. Da mesma forma, os ensaios eletroquímicos demonstraram uma maior suscetibilidade a corrosão em regiões próximas do centro da solda, em função da presença precipitados de Mg e de Si. Mesmo assim, com severidade corrosiva branda.

Palavras-chave: Liga de Alumínio Al6060-T5; resistência à corrosão; soldagem por fricção; FSSW; corrosão por imersão.

Resumen: Las aleaciones Al6060-T5 son ampliamente utilizadas en las industrias aeroespacial, naval y automotriz. Sin embargo, la soldadura convencional puede debilitar su resistencia a la corrosión. De esta forma, la soldadura por Friction Stir Spot Welding (FSSW) se convierte en una alternativa para reducir la zona afectada por el calor (ZAC) en la unión. En este contexto, este artículo evaluó soldaduras de láminas de Al6060-T5 en periodos de 336, 672 y 1008 horas de inmersión en NaCl al 3,5%. Para cada período, se evaluaron las láminas en cuanto a potencial de circuito cerrado (CCP), dureza Vickers, composición elemental y severidad corrosiva. Los resultados mostraron un aumento porcentual de Oxígeno (3 a 4%); Identificación de actividad corrosiva en la zona de mezcla. Asimismo, las pruebas electroquímicas demostraron una mayor susceptibilidad a la corrosión en regiones cercanas al centro de la soldadura, debido a la presencia de precipitados de Mg y Si. Aún así, con una severidad corrosiva leve.

Palabras clave: Aleación de aluminio Al6060-T5; resistencia a la corrosión; soldadura por fricción y agitación; FSSW; corrosión por inmersión.

Data de submissão: 20.04.2024
Data de aprovação: 06.12.2024

Identificação e disponibilidade:
(https://revista.univap.br/index.php/revistaunivap/article/view/4567,
http://dx.doi.org/10.18066/revistaunivap.v31i71.4567).

1 INTRODCTION

Earth's crust most abundant metal, aluminium, stands out in industrial applications. According the Brazilian Aluminium Association data bank, Brazil is the 12th producer of primary aluminium. With a production of 810.000 tons in 2022. Likewise, occupying the 3th world position in bauxite and aluminium producing; earning 140 billion BLR and generating a half of million jobs (Brazilian Aluminium Association [ABAL], 2023). The aluminium alloys properties combination of: low density, high corrosion resistance and high thermal and electrical conductivity. Allowing these steels alloys replacing, in several applications; highlighting structural applications in the automobile, aeronautics, and naval industries (Li et al., 2020). In this spectrum, Sharma et al. (2021) states that, despite adding alloy elements can be increase the mechanical strength, also affect other properties; such as corrosion resistance. For Copper adding example, Rana et al. (2012) and Ahmed et al. (2023) completes, the ion Cu^{2+} with potential reduction of E_{red} = 0.34, in contact with aluminium Al^{3+} (E_{red} = -0.166) causes aluminium oxidation. Where, the corrosion process is generally defined as a chemical/electrochemical deterioration (Gentil, 2023, p. 1524). Nevertheless, corrosion can also be associated with mechanical, or stress corrosion (Rao et al., 2016); acting onto material changing, such as wear, chemical or structural modifications, which modify the original component design.

Gentil (2023, p. 1524) points out that the corrosion it's a spontaneous process, occurring whenever there is a potential difference between the material and the environment. With this, from economic point of view, metals corrosion demands considerable losses; especially due to components replacing needing (Was et al., 2007). According to Koch (2017), this cost represents almost of 4% of global Gross Domestic Product (GDP), consumed by corrosion actions. This prospect shows the monitoring methods importance, in order to evaluate the corrosion process, as well as the material's corrosion resistance (Liz et al., 2015).

According to Eckermann et al. (2008) and Liz et al. (2015), the 6XXX series Al-Mg-Si alloys have high specific stiffness, good weldability, good formability, and corrosion resistance. As Osório et al. (2010) state its proprieties include a locate corrosion inducing either by pitting, intergranular or intragranular mechanisms, during the solidification process state, its proprieties include a locate corrosion inducing either by pitting, intergranular, or intragranular mechanisms during the solidification process or thermomechanical treatments. With its chemical composition, morphology and distribution of secondary phases disposed in the matrix, allowing this phenomenon. Where the Mg-Si precipitates are responsible for activating corrosion processes in Al-Mg-Si alloys, based on the evaluation of the electrochemical and compositional behavior of these precipitates (Liz et al., 2015). In this way, the distribution of intermetallic phases is a dominant feature when evaluating localized corrosion in these alloys, according to Birbillis and Buchheit (2005). Although, addressed studies on thematic morphological differences and distribution of intermetallic in the corrosion resistance are still scarce in the literature (Zeng et al., 2011). From these few studies, highlights the Ezuber et al. (2008) analyses, who's identified that the corrosion rate may vary throughout the process. Wherein the localized corrosion occurs in the first minutes of the electrochemical test; decreasing along the time. With this, the reduction in corrosion speed may be related to the passivation processes, even after the rupture of the passive film and active dissolution of the samples (Ezuber et al., 2008).

Under welding processes sphere, aluminium and its alloys have their peculiarities due to their high thermal conductivity and low melting point (Sharma et al., 2021). With this, welding difficulty, often results, in material using limitations in some specific applications. In this context, in 1991 The Welding Institute (The Welding Institute [TWI], 2024), developed a welding technique by friction and mechanical stirring (Friction Stir Welding - FSW); appliable not only to aluminium, but also to steels, dissimilar and non-similar metals. Where, the FSW process involves intense plastic deformation and frictional heat generation; with welding performing by non-consumable high hardness tool and the part to be welded interaction. With the tool being rotating and translating to make the weld bead. In the next time, variations emerged from this process, such as the Friction Stir Spot Welding (FSSW) process, such as the Friction Stir Spot Welding (FSSW) process; which differs from the FSW process in that the tool has no translation movement. In this horizon, Rosento et al. (2011) explain that the FSSW consists of three distinct steps: namely plunging, stirring and retracting. Where, the tool rubbing against the surface plates generates heat, producing a solid-state bonding between them, arranged in the lap configuration. Next, a downward movement spinning tool, first plunges into the upper plate, then penetrates the lower plate with a certain depth. After, this tool rotates at a fixed location (for a specified duration), allowing both plates into a fusion (Rosendo et al., 2011). With this, occur materials jointing (in the solid state), avoiding deleterious defects due to high temperature; and allowing the structural joint between 6XXX aluminium alloys (Vale et al., 2018; Kumar et al., 2019).

In this context, Lumsden et al. (2003) studied the corrosive behaviour of AA7050-T7651 aluminium alloys welded by the FSSW process. Evaluating each welded joint region, separately, through potentiodynamic polarization curves. Comparing potentials with base metal; under a 3.5% NaCl aqueous solution. Concluding that the diffusion and heat affected zones (HAZ), presents high negative potentials, allowing most intergranular and pitting corrosion occurrence. In this way, FSSW demands more in-depth studies about the durability of the welded material in service life; in order to achieve wider its industrial application. Thus, this paper reports the microstructural evaluation and corrosive behaviour of a 6060-T5 aluminium alloy welded by FSSW. Aiming a welding behaviour investigating, under a prone corrosion environment; allowing the planning of alternatives to provide greater reliability to this welding process and expanding its applications.

2 EXPERIMENTAL PROCEDURES

2.1 SPECIMENS FABRICATION: MACHINING AND WELDING

For this scientific investigation were used 6060-T5 aluminium alloy plates. With dimensions of: 3.2mm (thick l_1'), 100mm (long l_2) and 25mm (wide l_3). These dimensions attend International Organization for Standardization (ISO:14273, 2016) specification for welded specimens. The Figure 1[A] show the specimen schematic draw. Where the Lower Plate (LP) and Upper Plate (UP) were highlighted; with its EDS composition in [B].

Figure 1 - Schematic view of specimens and its EDS composition.

[A]

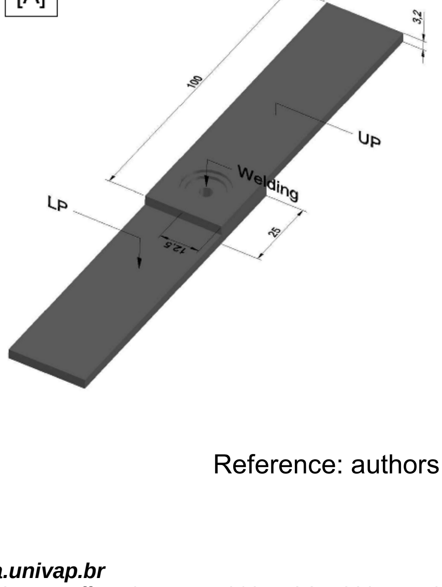

[B]

Elements	% Weight
Si	0.45
Fe	0.19
Cu	0.06
Mn	0.08
Cr	0.003
Zn	0.01
Ti	0.03
Al	98,52
Others	0.02

Reference: authors, 2024.

These plates were machined from 25X25X120mm billets; using a computational numeric control machining (CNC). Next, sanded (220-1200grit sandpapers), polished (alumina of 1μm of grit) and cleaned using an ultrasonic bathtub for 20 min, 25°C, 20 kHz into acetone. Sequentially, the plates were welded according Table 1 parameters (Aita et al., 2020). To this end, was used a CNC machine with plates fixed according to Figure 2[A] configuration and a welding tool (WT); made from M2 steel; with geometry detailed in Figure 2[B]. Parallelly, temperature was monitored during the welding process, with thermocouples (TJ1 and TJ2) distributed according Figure 2[2].

Table 1 – Parameters for FSSW.

Parameters	Variable	Unit	Value
WT's rotation speed into specimen	S_w	**RPM**	**1500,00**
WT's Pin to shoulder penetration speed into specimen	S_p	**mm/min**	**120,00**
WT's dwell time into specimen	t_s	**s**	**4,00**

References: authors, 2024 based on Aita et al. (2020).

The temperature acquisition was interpreted by an HBM/Spider 8 controlled computer; using a 50Hz signal conditioner. In addition, the axial load was measured using a load cell; obtaining the Figure 3 graph. Where the axial load increases, while the tool enters into the plate. Increasing even more when the tool "shoulder" touches the UP surface and reaches to the maximum at the end penetration. Next, decreasing from this moment and during the dwell time, until the process end.

Figure 2 – Photography and schematic of FSSW development procedures.

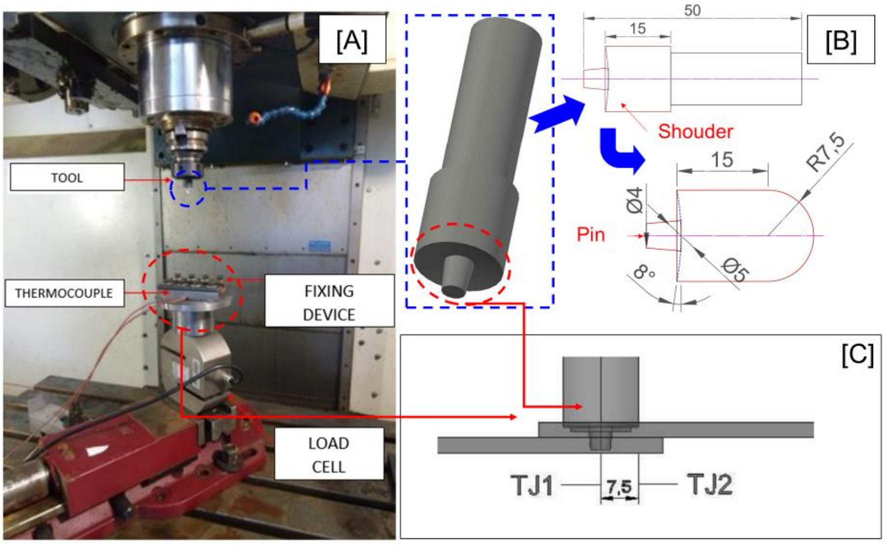

Reference: authors, 2024.

Figure 3 – Load evolution during the welding process.

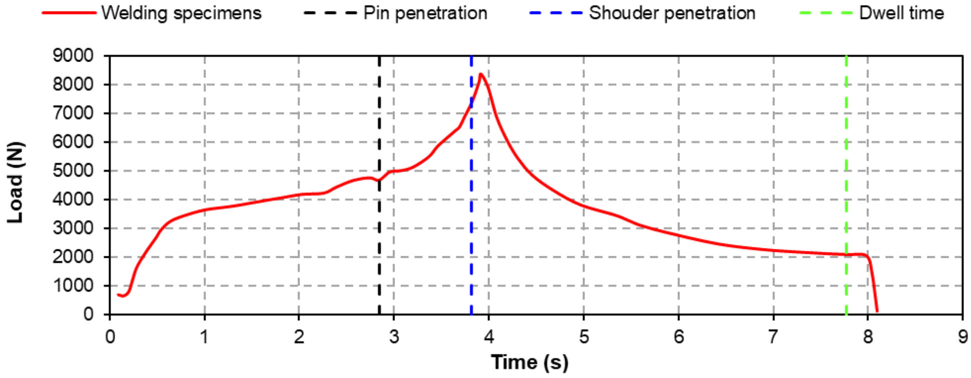

Reference: authors, 2024.

The FSSW process produced 13 specimens for testing. Of these, 4 weren't subjected to immersion corrosion test (ICT). Of these four, 3 were used as "control" (no testing) and 1 was subjected to linear polarization resistance (LPR) test. The nine remaining were divided into 3 groups subjected to ICT. Where, each group remained immersed into aqueous NaCl solution for a certain period of time, as Figure 4 flowchart shown, according its terminology by immersion time.

Figure 4 – Flowchart of FSSW preparation procedures up to definition of ICT specimen groups.

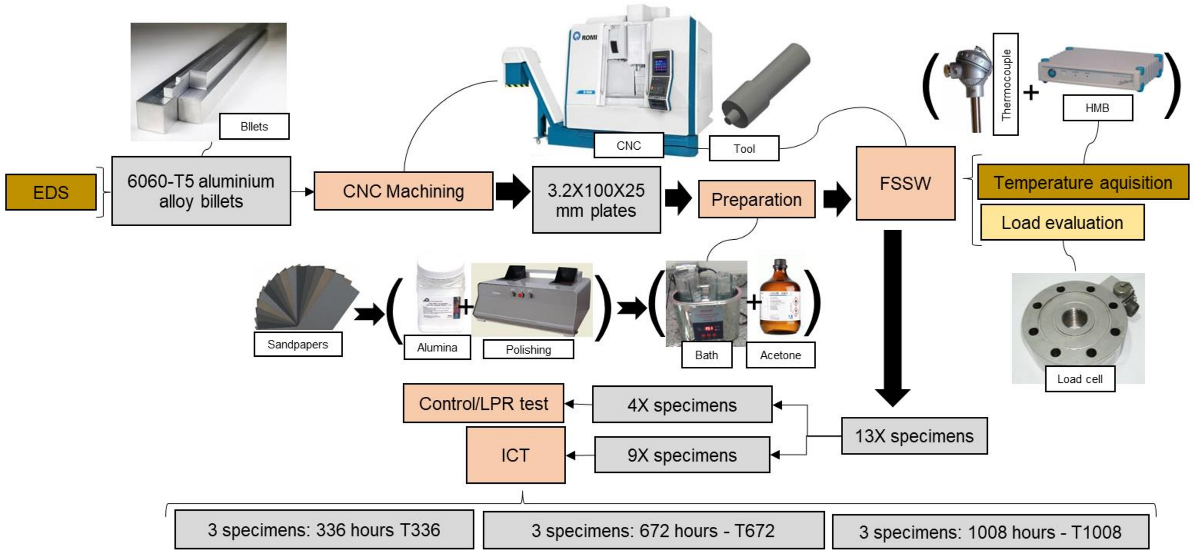

Reference: authors, 2024.

2.2 IMERSION CORROSION TEST (ICT)

Initially, was prepared the electrolyte solution; using 6.33g of NaCl (99%-purity) into 2 litters of distilled water. The obtained pH of 6.5 was considered to be within the American Society for Testing & Materials (ASTM:G44, 2021) criteria; classifying the electrolyte as close to seawater.

Parallelly, specimens were covered by a galvanoplastic tape; exposing only the weld region for corrosion attack (Figure 5[A); and weighed. Next, 5 and 4 specimens (randomly chosen) were inserted into two 3-liter glass vessels with electrolyte completely immersing these specimens. Finally, the vessels were oven placed; at 30°C of temperature; remaining covered, but not sealed from as Figure 5[B] shown.

Figure 5 – Photos of specimen tape covered and vessels into oven during ICT.

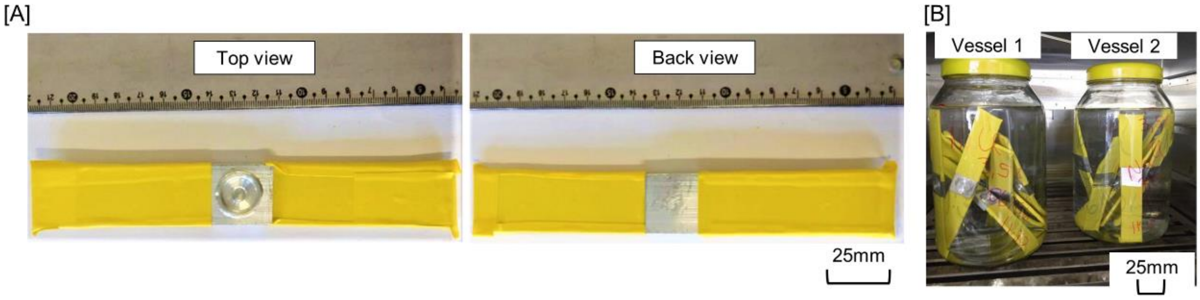

Reference: authors, 2024.

The open circuit potentials (OPC) of each specimen group were measured; every 14 days after its immersion; according to Rodrigues’s (2012, p. 117), Bertouli's (2012, p.112) and ASTM: G44 (2021) recommendations. Likewise, the pH was also daily monitored, as Figure 6[A] illustrates. For OCP measurements, was used an electrode calomel saturated (ECS) and the specimen itself as the working electrode connected to Multimeter, as Figure 6[B] shows. Observing that for each measurement, was adopted 30min for stabilization. In sequence, these specimen group were withdrawn from solution and identified. Next, the tapes were removed and washed with distilled water, according to ASTM: G-1 (1999) recommendations.

Figure 6 – Illustrative photos of pH and OCP measurement procedures for ICT.

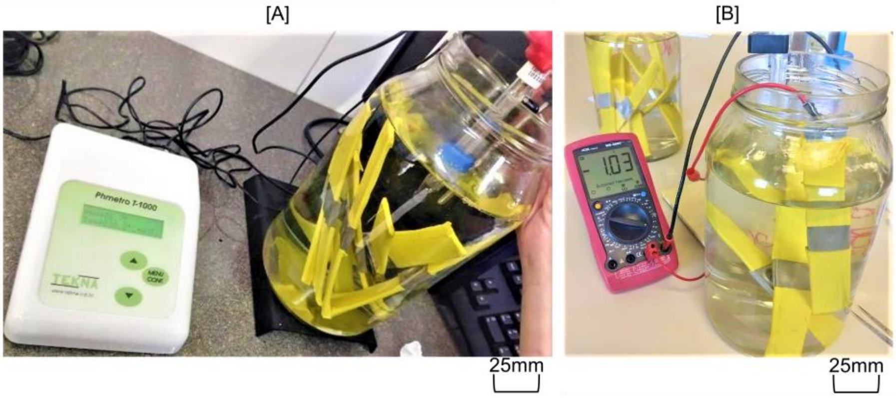

Reference: authors, 2024.

2.3 LINEAR POLARIZATION RESISTANCE TEST (LPR)

The LPR test also aimed polarization curves; through OPC measuring. Where the OCP; also called E_{corr}, was obtained. However, in the LPR test (unlike the ICT), the OPC was determined for 3 regions of a specimen cross-section (not subjected to ICT). Likewise, pitting E_{pit} and density i_{pit} potentials were obtained. As well, as anodic β_a and cathodic β_c Tafel slope coefficients (Bard & Faulkner, 2000).

Initially, two sections were cut: main section (MS) and base section (BS). For MS, 2 parallel sectional cuttings were made 0.5mm from the middle of the specimen weld button and apart from 10mm, as Figure 7[A] show. For BS, a 10X3.2X10mm parallelepiped was extracted from the specimen UP end, as Figure 7[A] also shows. Next, MS and BS were embedded in Bakelite and metallographically prepared.

The areas were delimited as: UP1, UP2 and LP1, as Figure 7[B] show. In which the areas UP1, LP1 and UP2 correspond respectively to: Mixing (or welding) zone of the upper and lower plate (MZ) and the interface between the Thermally Affected Zone (HAZ) and the MZ of the upper plate (HAZ/MZ). Where, the working electrode was fixed for E_{corr} measuring; while the rest of MS was isolated using a transparent enamel, as Figure 7[C] show. For comparative, BS's E_{corr} was also measured.

Figure 7 – Schematics for SM and BS withdraw locate and SM masking for UP 1 and 2 and LP1.

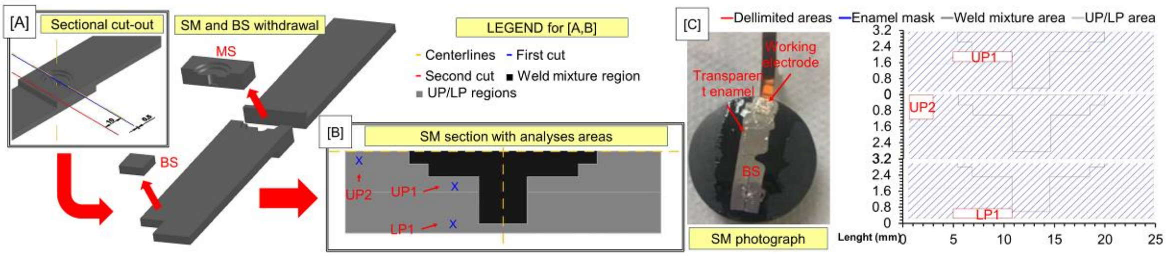

Reference: authors, 2024.

The LPR tests were performed with 3.5% NaCl electrolyte, prepared analogously to the ICT. With set-up imbued with an open-circuit connected to a conventional electrochemical cell containing: electrode of $Ag/AgCl_{KClsat}$ as reference, 6cm² platinum sheet (counter electrode) and BS/MS areas as working electrode, as Figure 8[A] show; protected by a grounded Faraday cage, as Figure 8[B] show.

Figure 8 – Photographs of the LPR test set-up detailing the electrolytic cell.

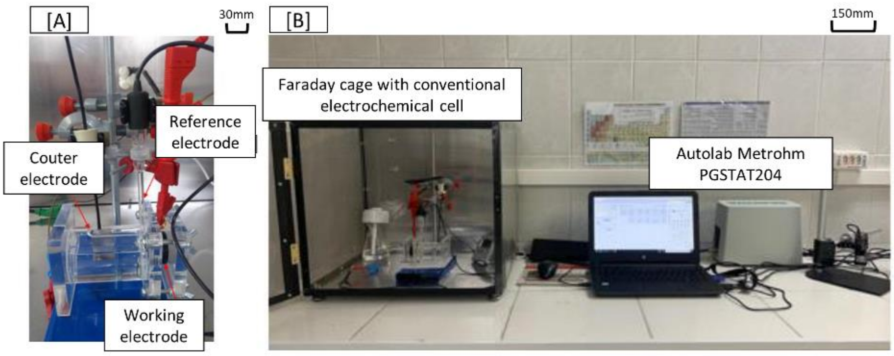

Reference: authors, 2024.

The regions were individually potentiostat (in potentiostatic mode) connected, acting as a working electrode. Thus, for linear polarization technique, the OCP was ±0.02 + E_{corr} variated (ΔE_{corr}) in relation to E_{corr} with an associated current density "i" (A/m²); for each MS and BS region; at a scanning rate T_{corr} of 0.02 mV/s. Where, each E_{corr} measurement was determined after 30 minutes of ΔE_{corr} (for stabilization). Next, data was processed determining also E_{pit} and i_{pit} values. Sequentially, this databank was pos-processed obtaining potential curves were plotted; determining values of interest. In addition, the corrosion rate (£) in mm/year was estimated using an extrapolation; using β_a and β_c Tael's slopes.

2.4 ANALYSIS

After ICT, the specimen groups were prepared, according to Figure 9 flowchart for Vickers micro-hardness (MHV) and SEM/EDS analysis.

Figure 9 – Specimens preparation flow-chart for analysis.

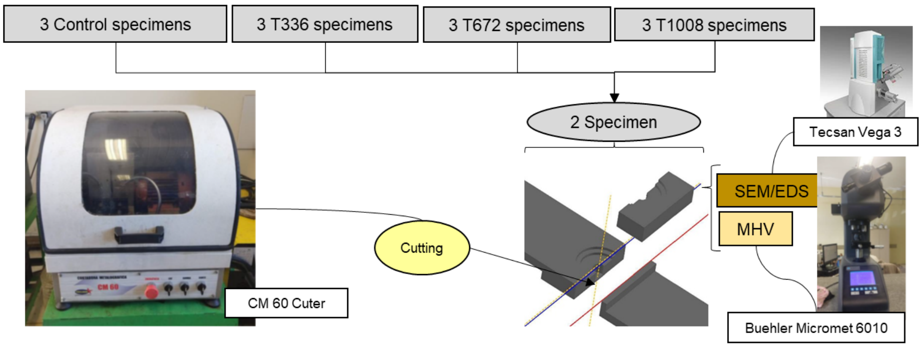

Reference: authors, 2024.

The MHV test was evaluated with load of 200g for 10s. Aiming the evaluation of corrosion interference on welded joints hardness. For this purpose, were made approximately 40 indentations; spaced by 500μm (*id*). Under the all l_3 middle of UP (i_{UP}) and LP (i_{LP}) sections, as Figure 10 show.

Figure 10 – MHV test indentations localization under UP and LP sections.

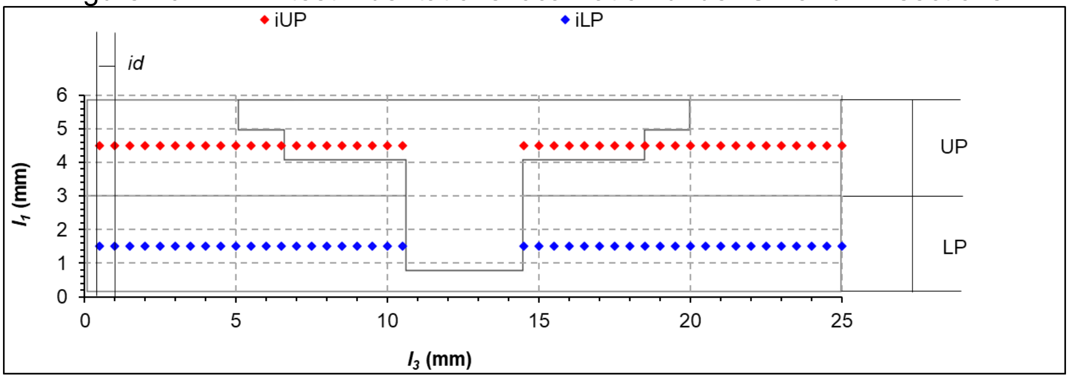

Reference: authors, 2024.

The SEM analysis, in other hand, initially aimed the weld quality investigation; evaluating control's weld uniformity and defects. To this end, magnified images (20X to 53X) were taken of the total MS section. In addition, the LP1, UP1 and UP2 regions, with an extra "LP2" region (corresponding to the LP's HAZ-MZ), were also analysed, obtaining elemental composition from these regions by EDS.

In sequence, SEM micrographs (20X increase) were taken, in order to detect structural anomalies of ICT and control specimens. Other SEM (500 to 1000X increases) micrographs were also taken to classify the pitting corrosion severity. For this purpose, the procedures of ASTM: G46 (2021), were carried on; considering the pitting areas and lengths measurements, in relation to Figure 11[A]'s matrix. Where, the valuation of 1 (insignificant) to 5 (severe) are attributed, according the density (dots/m²), area (mm²) and depth (mm) pitting. Additionally, the pitting morphologies were also visually classified; comparing to European Normatization Comitee (EN:11463 British Standards, 2008)'s matrix of Figure 11[B].

Thus, the classification was analytically and visually carried out; considering the pitting of section's MZ and HAZ-MZ with the last corresponding to a partially welded zone (PWZ). In addition, were performed EDS for evaluate Al-Mg-Si changes.

Figure 11 – ASTM: G46 and EN:11463 's diagram for corrosion classification.

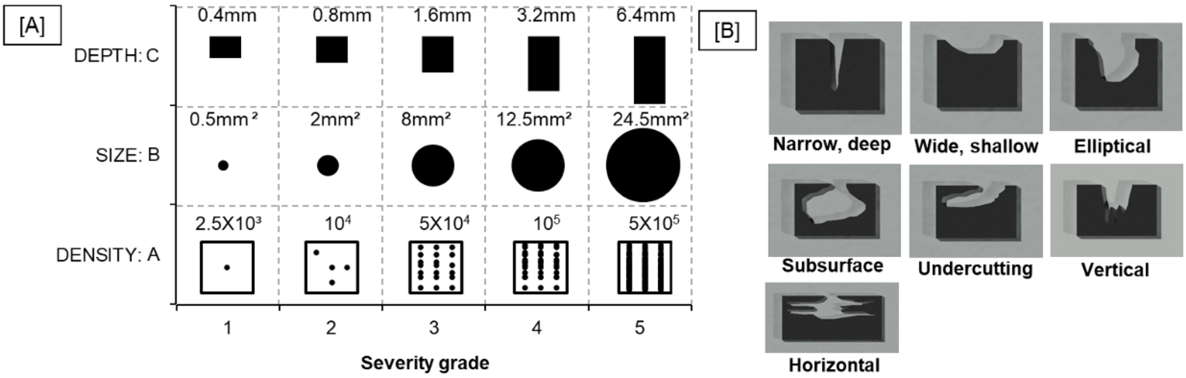

Reference: authors, 2024.

3 RESULTS AND DISCUSSIONS

3.1 FSSW specimen properties

The J1 and 2 thermocouples registered a tool pin temperature peak of 241°C. According to Li et al. (2020), sufficient to 6060-T5 aluminium alloy series melting (~160°C). The peak tool "shoulder" temperature (142°C), non the other hand, was in line with other studies (Aita, 2017), as Figure 12 [A] show. Sharma et al. (2021) explain that this occurrence contributes to weld uniformity, ensuring weld spreading and mixing. In fact, as Figure 13[B] photo; shows, was noted a welding uniformity imbued with apparent anchoring between UP and LP. Where a notorious constatation of tool pin's hole, as well as burrs occurrence, due to material spreading.

Figure 12 – Results of thermal evaluation of the specimen and tool during the FSSW.

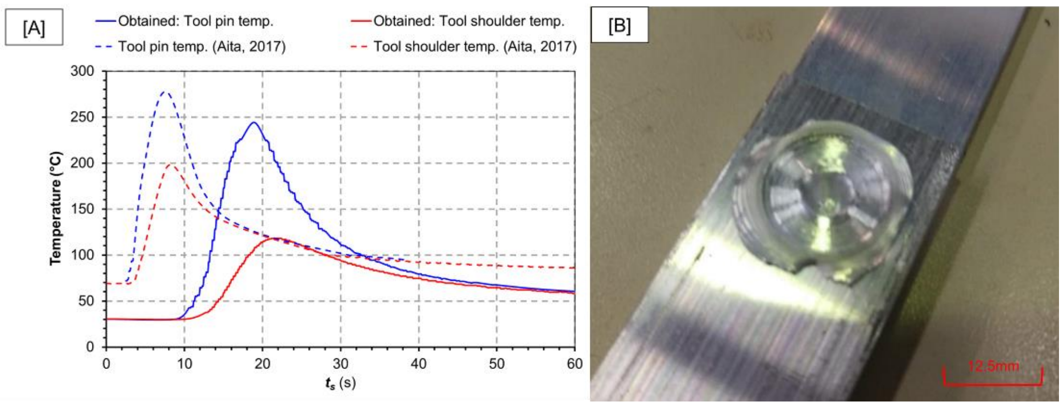

Reference: authors, 2024.

This apparent UP/LP anchoring is confirmed by Figure 13[A] SEM (20-53X) micrographs; with a notable melted material uniformity, observed between the UP/LP plates. In addition, presenting absence of cracks and/or macro-pores by visual observation. Furthermore, EDS by regions corroborate these assertions, as Figure 13[B] show. With this, the MHV profile shows an expected alloy hardness behaviour.

In addition, for MHV, weld process implied a joint region hardness peak, as Figure 13[C] show. According to Sharma et al. (2021), the hardness peak on plates mix region are characterized by the HAZ influence; allowing oxygen capture with consequent aluminium oxides increasing, which are harder.

Figure 13 – Results of SEM/EDS analysis of FSSW.

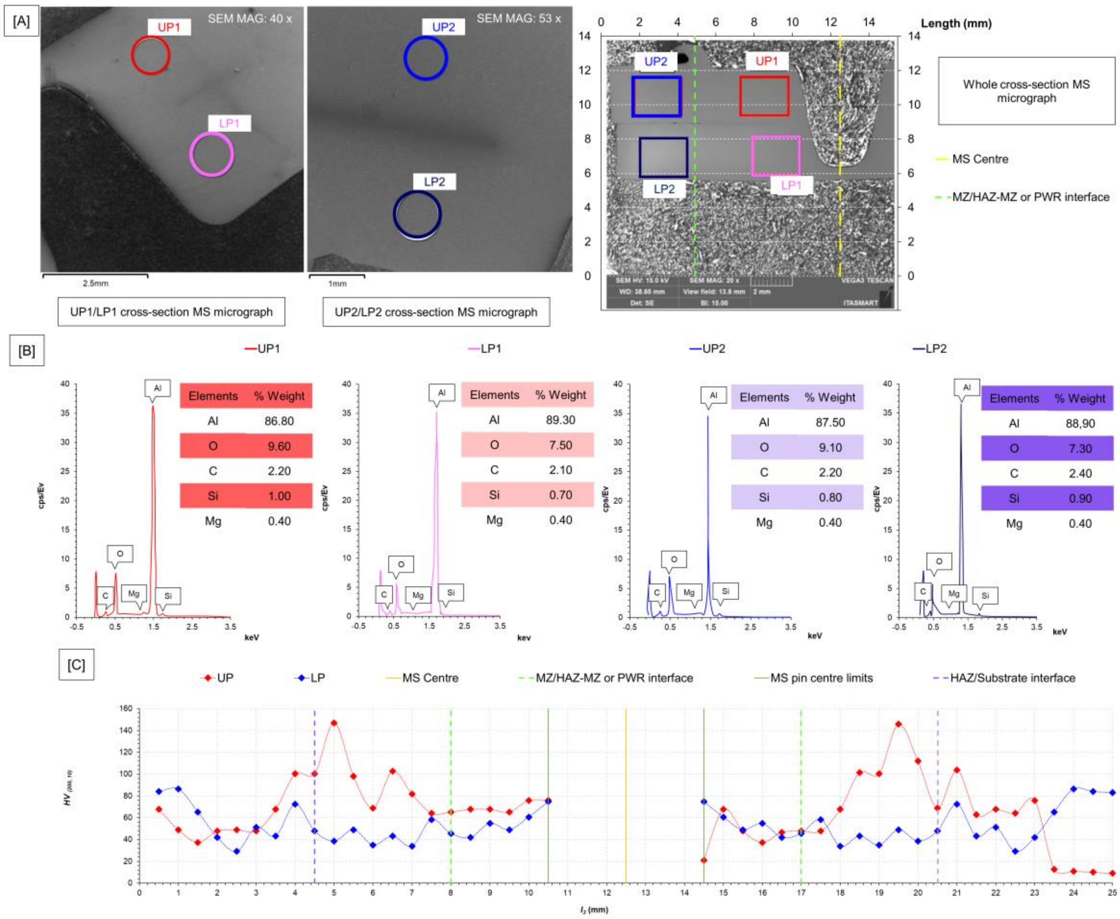

Reference: authors, 2024.

3.2 FSSW specimen properties due to corrosion immersion attack

The SEM micrographs (20X magnification) of MS show visual gradual corrosion by-products increase; as a function of immersion time increasing (336-1008h), as shown in Figure 14[A]. Where the presence of small white dots, nearing the MS centre, were noted. Similarly, darker regions were also observed from nearing the UP/LP contact region (PWR/Substrate). These observations indicate the Mg or Mg and Si compounds formation; a typical corrosion by-product of Al alloy (Bousquet et al., 2011). At the same a gradual oxide increasing was observed from the MS's UP1 and 2 and LP1 and 2 regions, according to EDS of Figure 14[B].

Figure 14 – Results of MS's SEM/EDS and XRD analysis after corrosion immersion attack.

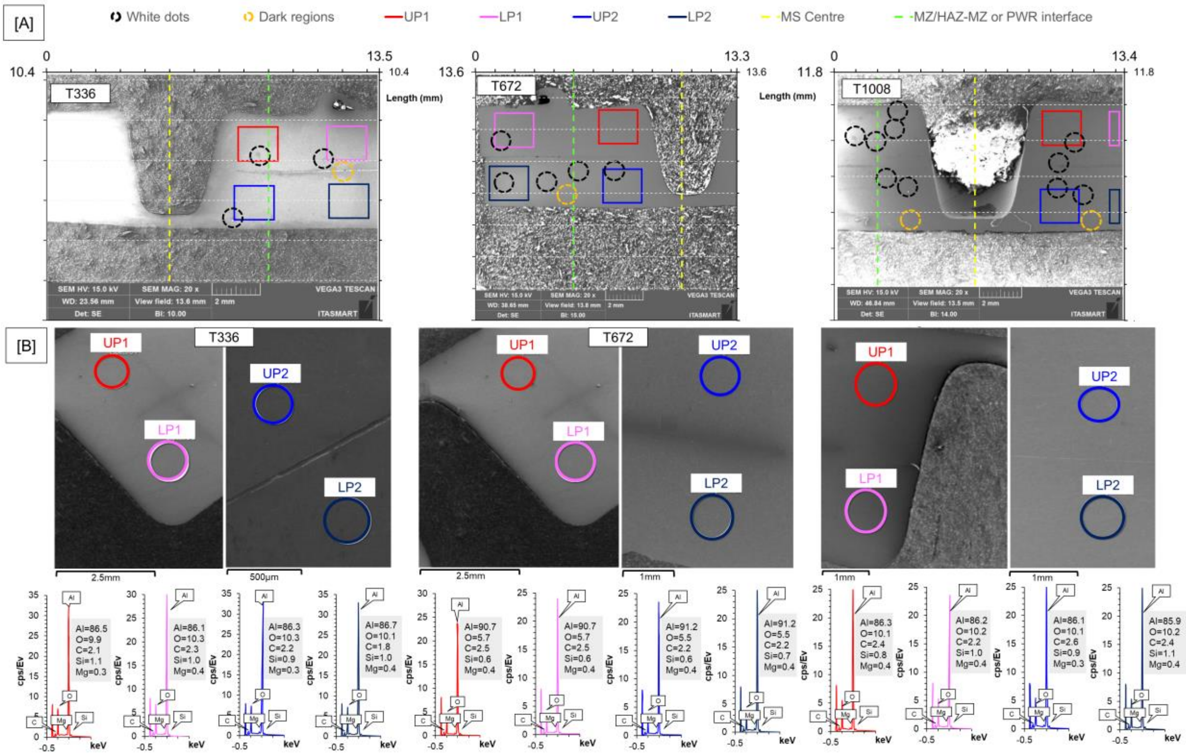

Reference: authors, 2024.

Liang et al. (2018) and Bousquet et al. (2011) point out that SEM/EDS results; aka these of Figure 14[A, B]; indicate the pitting and intergranular corrosion local occurrence. In addition, more specifically, under PWR/Substrate interface regions. These discussions justified the pitting severity and morphology analysis; with the specimens presenting a pitting predominance of wide and broad shallow morphology; by comparative analysis between Figure 11[B] and micrographs. Likewise, the specimens present a pitting size with less than 0.5mm² (B1); as Figure 15 show. With this, the corrosive severity was considered very mild for all immersion times; according to Figure 11[A] matrix. Thus, despite the gradual increase of Si and MgSiMg, as immersion time function, the severity of pitting remained mild.

Figure 15 – Results of the pitting analysis.

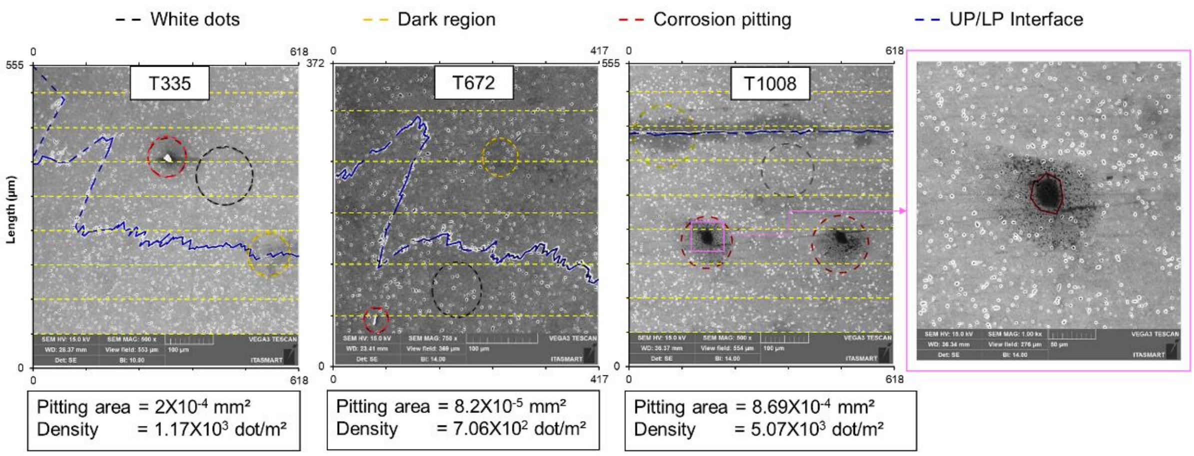

Reference: authors, 2024.

According to Liao and Wei (1999) and Callister Jr. and Rethwisch (2014), the passive film rupture; by aggressive ions; may be related to Si and Mg and Si dissolution. In this way, Jesuíno et al. (2001) and Ackermann et al. (2008) point out the role of tthese intermetallic compounds acting as a corrosion-activator. Therefore, the Dehnavi et al. (2014) assertions are confirmed; due to this passivation process occurring in the specimens. Likewise, the MHV properties also corroborate these assertions, as Figure's 16 show. Where an absence of significant changing were noted between LP specimens. Nevertheless, at the UP region, there was an MHV decrease in PWR/Substrate interface regions; where higher concentrations of Mg and Si precipitates were visually noted.

Figure 16 – Results of MHV test of MS's samples after immersion corrosion test.

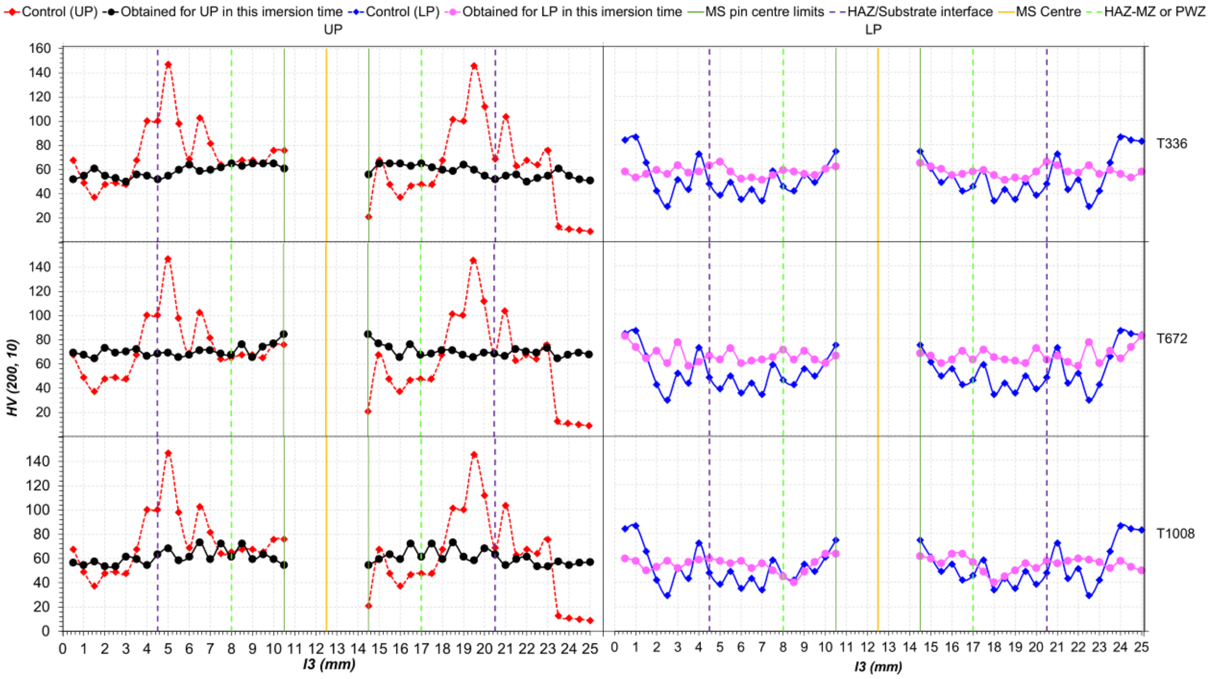

Reference: authors, 2024.

In this context, Lumsden et al. (2003), Fonda et al. (2009) and Bousquet et al. (2011) highlight the welding heat inputting benefits the recrystallization process. In other words, HAZ effect make weld region more hardness, due to oxides increasing, with consequent more susceptibility corrosion attack, due to oxygen increasing facilitates the passivating film breakdown. As a result, UP had a by-products higher occurrence, due to welding tool more significant contact. In this way, occur a MHV reducing in this region, due to low-hardness of these by products in relation to aluminium alloy. In the same way, the Mg and Si presence increases the impact under electrical potential (E_{corr}) increase, as Figure's 17 graph shown. According to Bousquet et al (2011), a E_{corr} increasing may indicates the corrosion increment; considering Mg and MgSi ions reducing the sample electrical resistivity. As a result, the more significant the difference in corrosion severity, more potential variations.

Figure 17 – Results for ICT in relation to OCP (E_{corr}) and immersion time.

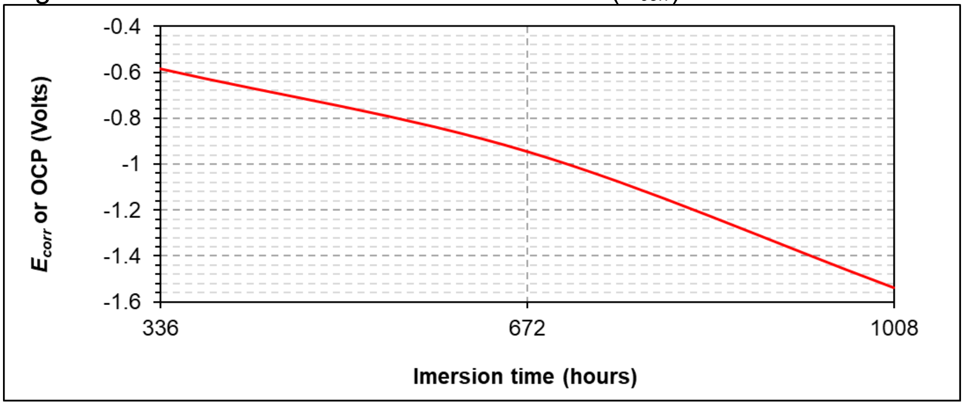

Reference: authors, 2024.

3.3 Potentiodynamic properties of FSSW

The LPR's test polarization graph (or potentiodynamic polarization) of Figure 18 showed 'less positive E_{corr}' values, as well as 'higher I' values. On the other hand, UP2 and BS showed 'less positive E_{corr}' values, as Table 2 details. In addition, BS stabilized with a very low E_{corr} (or 'less noble'); in comparison with the other regions. However, with a difference between these regions values lower than 0.3 V; indicating a little accentuated polarization effect due to regions coupling by welding.

Figure 18 – Results of the LPR test throughout polarization curves obtained.

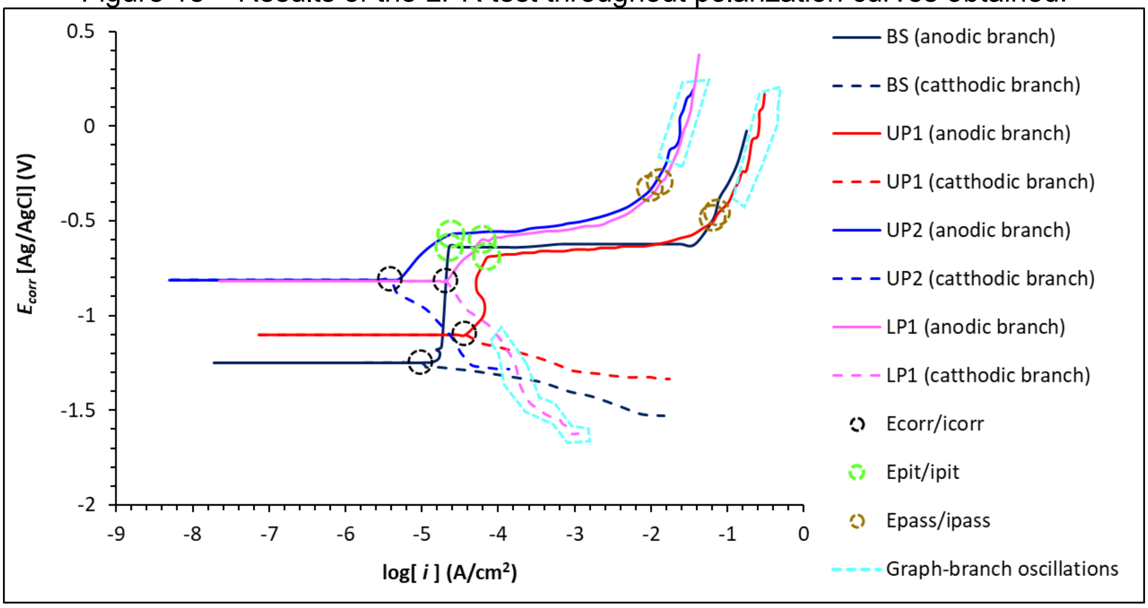

Reference: authors, 2024.

Table 2 – Obtained results of LPR test for Control sample regions.

Regions	E_{corr} V	i_{corr} A/cm^2	E_{pit} V	i_{pit} A/cm^2	E_{pass} V	i_{pass} A/cm^2	β_a T^{-1}	β_c T^{-1}	£ mm/year
BS	**-5.01**	**-1.25**	**-0.64**	**-4.64**	**-0.49**	**-1.18**		**-0.77**	**0.02**
UP1	**-1.10**	**-4.43**	**-0.69**	**-4.14**	**-0.46**	**-1.13**	**-3.07**		**1.82**
UP2	**-0.81**	**-5.41**	**-0.57**	**-4.62**	**-0.33**	**-2.00**		**-0.77**	**0.33**
LP1	**-0.82**	**-4.68**	**-0.60**	**-4.21**	**-0.30**	**-1.88**	**-3.07**		**1.22**

Reference: authors, 2024.

According Bard and Faulkner (2000), anodic branches disturbances (graph region with less negative E_{corr}) are related to pits and corrosion products, formation and dissolution. With an observation of a pre-passivation effect under the samples; characterized by an increase of initial E_{corr}; also called E_{pass}, with an associated initial i density; also called i_{pass}. Next, to a certain point; for all analyses; occur the passive film breakage under a certain E_{corr}; or E_{pit} (with an associated density or i_{pit}). Followed by material active dissolution, until for its repassivation. Thus, samples with 'more positive E_{pit}' values get a greater corrosion resistance, than 'less positive E_{pit}'. The branch disturbances (graph region with more negative E_{corr}), on the other hand, are characterized by diffusion processes. With this, aerated environment is related to corrosion's oxygen rate diffusion. Where, microbubbles releasing promote these graph-branch oscillations.

In this context, this mechanism explains the "Control" sample's results; for all regions. Where, as Figure 19 shows, even after the oxide layer breakdown, occur the sample's region passivation. In the same way characterized by a E_{pit} increasing associated with i_{pit} less-changing; until reaching to the highest E_{corr} (OCP) values. With this, a self-protection region tendency was noted. As consequence occur the surface rapid-passivation, with an E_{pit} high increase, followed by film rupture.

This process confirms the Liang et al. (2018) and Bousquet et al. (2011) assertions; in face of UP1, UP2 and LP1 SEM/EDS results. Where, the repassivation phenomenon, highlighted by Dehnavi et al. (2014), may be occurring. In this context, Liao and Wei (1999) point out that the formation of 'metastable pits' occurs, that is, pits that nucleate and repassivate. This explains the high concentration of corrosion products in these regions (or PWR/Substrate interface zone), without a considerable density of pits (A-1, B-1 or very light corrosion severity).

Assis (2017) highlight that the top-plate's greater tool contact, impute highest temperatures at this region; occurring the well-known dynamic recrystallization phenomenon in the mixing zone region. Where the mechanical deformation induces a microstructure refining in the area; with oxides increasing. In this way, UP2 and MS (far from the mixing zone) are more corrosion resistant, than UP1 and LP1. This results in higher i_{corr} values in these regions; indicating a high corrosion kinetics. Thus, triggering higher £ values for the PWR/Substrate interface; according to Tafel's extrapolation. Where the UP1 and LP1 presented 1.22 and 1.82 mm/year (respectively), against 0.4 and 0.02 mm/year of UP2 and MS, respectively. A difference of 4-91 times higher, as Table 2 also shown. Nevertheless, as Gentil (2023) points out, the corrosion rate (£) analysis, could be only individually considered, under a uniform corrosive attack. With this, although; according to UP1, UP2 and LP1 SEM images; the occurrence of localized pitting corrosion and signs of intergranular corrosion were evident, due to the presence of corrosion products, this being a criterion to be observing £ values with other variables, but not individually.

4 FUTURE SCOPE AND CONCLUSIONS

4.1 Future scope

From analyses, new research fronts were identified. Which are also explored little. Thus, this paper identified new research opportunities:

- Conduct intergranular corrosion tests, according to ASTM: G110 (2022); evaluating welded joint mechanical and chemical properties;
- Re-conduct immersion test varying the electrolyte concentration and its temperature and composition;
- Conduct salt spray corrosion test, according to ASTM: B117 (2019), to assessing welded joint mechanical behavior;
- Verify the tool rotation speed influence (FSSW processing) under the located corrosion of welded regions;
- Perform welded joint electroanalytical analysis, using cyclic voltammetry with same electrolyte concentration; evaluating related coupled-reactions to electrochemical processes, such as repassivation process;
- Evaluate the MS topography after the immersion corrosion process, using Atomic Force Microscopy (AFM); evaluating the pitting depth into AA6060-T5 alloy intermetallic.

4.2 Conclusions

In face of obtained results from the analysis carried out, the following conclusions can be drawn:

- The immersion test samples presented localized corrosion, with pitting and corrosion products increasing as the test time increased;
- According to the SEM analysis; in face of ASTM: G46 (2021) diagram; the corrosion severity (for all immersion times) was classified as mild;
- EDS analysis shown an existence of corrosion process, due to Oxygen concentration variations; as function of with the longest of immersion time. Where, the direct relationship between the alloying elements and localized and intergranular corrosion occurrence was evident;
- PWR/Substrate interface SEM analysis showed Mg and Si precipitates dissolution; resulting from corrosion process and products. Where, for T1008 sample, small pits were identified in the partially welded region;
- The potentiodynamic curves indicated an UP's highest corrosion prospection, due to mixing zone effect; presenting a £ of 1.82 mm/year. Where the presence of Mg and Si precipitates can trigger the localized corrosion process, as they have undergone preferential dissolution; showing anodic behaviour in relation to the other alloy components.

REFERENCES

Ahmed, S., Anwar, S., Islam, S., & Arifuzzaman, M. (2023). Experimental study on the effects of three alloying elements on the mechanical, corrosion and microstructural properties of aluminium alloys. *Results in Materials*, 20(2023), 100485, https://doi.org/10.1016/j.rinma.2023.100485

Aita, C. A. G. (2017). *Study of the mechanical performance of friction stir spot welding (FSSW) joints of AA6060-T5 alloy*. [Thesis Master on Engineering], Materials Technology, Strict Sensu Postgraduate Degree in Engineering at the Federal University of Pampa.

Aita, C. A. G., Goss, I. C., Rosendo, T. S., Tier, M. D., Wiedenhöft, A., & Reguly, A. (2020). Shear strength optimization for FSSW AA6060-T5 joints by Taguchi and full factorial design. *Journal of materials research and technology*, *9*(6), 16072-16079, https://doi.org/10.1016/j.jmrt.2020.11.062

American Society for Testing & Materials. (2019). ASTM B117-85: *Standard Practice for Operating Salt Spray (Fog) Apparatus*.

American Society for Testing & Materials. (2022). ASTM G110-92: *Standard Practice for Evaluating Intergranular Corrosion Resistance of Heat Treatable Aluminium Alloys by Immersion in Sodium Chloride + Hydrogen Peroxide Solution*.

American Society for Testing & Materials. (1999). ASTM G1-90: *Standard Practice for Preparing, Cleaning, and Evaluation Corrosion Test Specimens*.

American Society for Testing & Materials. (2021). ASTM G44-21: *Standard Practice for Exposure of Metals and Alloys by Alternate Immersion in Neutral 3.5 % Sodium Chloride Solution*.

American Society for Testing & Materials. (2021). ASTM G46-21: Norma: *Standard Guide for Examination and Evaluation of Pitting Corrosion*. West Conshohocken, 2021.

Assis, C. L. (2017). *Study of the corrosion behaviour of friction stir welded (FSW) aluminium alloys using global and local electrochemical techniques*. [Thesis on Sciences], Chemistry Engineering, Polytechnic School of the University of São Paulo.

Associação Brasileira de Alumínio. (2023). *Anuário Estatístico do Alumínio ABAL - 2022* (1. ed.).

Bard, A. J., & Faulkner, L. R., (2000). *Electrochemical Methods: Fundamentals and Applications* (2. ed.). Wiley.

Bertouli, P. T. (2012). *Development and characterization of a polyester-based powder paint containing montmorillonite functionalized with silane*. [Thesis Master on Process Engineering Processes and Technologies], Engineering Process and Technology, Engineering of Processes and Technologies at the University of Caxias do Sul.

Birbillis, N., & Buchheit, R.G. (2005). Electrochemical Characteristics of Intermetallic Phases in Aluminium Alloys. *Journal of The Electrochemical Society*, *152*(4), B140-B151. https://doi:10.1149/1.1869984

Bousquet, E., Poulon-Quintin, A., Puiggali, M., Devos, O., & Touzet, M. (2011). Relationship between microstructure, microhardness and corrosion sensitivity of an AA 2024-T3 friction stir welded joint. *Corrosion Science*, 53(2011), 3026–3034. http://dx.doi.org/doi:10.1016/j.corsci.2011.05.049

British Standards. (2005). *EN 11463-08*: *Corrosion of metals and alloys — Guidelines for the evaluation of pitting corrosion*. British Standards Institution

Callister Jr., W. D., & Rethwisch, D. G. (2014). *Materials Science and Engineering an Introduction* (9.ed.). Willey.

Dehnavi, D., Liub, X. Y., Luanb, B. L., Shoesmith, D. W., & Rohani, S. (2014). Phase transformation in plasma electrolytic oxidation coatings on 6061 aluminum alloy. *Surface & Coatings Technology*, 251(2014), 106–114. http://dx.doi.org/10.1016/j.surfcoat.2014.04.010

Eckermann, F., Sutera, T., Uggowitzerb, P. J., Afsethc, A., & Schmutza, P. (2008). The influence of MgSi particle reactivity and dissolution processes on corrosion in Al–Mg–Si alloys. *Electrochimica Acta 54*, (2008), 844–855. https://doi:10.1016/j.electacta.2008.05.078

Ezuber, H., El-Houd, A., El-Shaweshet, F. (2008). A study on the corrosion behaviour of aluminium alloys in seawater. *Materials and Design*, 29(2008), 801–805. https://doi:10.1016/j.matdes.2007.01.021

Fonda, R. W., Pao, P. S., Jones, H. N., Feng, C. R., Connolly, B. J., & Davenport, A. J. (2009). Microstructure, mechanical properties, and corrosion of friction stir welded Al 5456. *Materials Science and Engineering A*, 519(2009), 1–8. https://doi:10.1016/j.msea.2009.04.034

Gentil, V. (2023). *Corrosão*. (7. ed.). LTC.

International Organization For Standardization. (2000). ISO 14273: *Resistance welding — Destructive testing of welds — Specimen dimensions and procedure for tensile shear testing resistance spot and embossed projection welds*. ISO.

Jesuíno, G. A., Ribeiro, L. M. F., Nakazato, R. Z., Codaro, E. N., & Hein, L. R. de O. (2001). Mechanical Properties and Corrosion Resistance of Ti-4Al-4V Alloy Obtained from the Recycling of Ti-6Al-4V Alloy. *Materials Research*, *4*(2), 63-69, 2001.

Koch, G. (2017). Cost of corrosion. In A. M. El-Sherik (Org.), *Trends in Oil and Gas Corrosion Research and Technologies* (pp. 3–30). Elsevier. https://doi.org/10.1016/B978-0-08-101105-8.00001-2

Kumar, A., Arora, K. S., Gupta, R. K., & Harmain, G. A. (2019). Investigation on interface morphology and joint configuration of dissimilar sheet thickness FSSW of marine grade Al alloy. *Journal of the Brazilian Society of Mechanical Sciences and Engineering*, *41*(381), https://doi.org/10.1007/s40430-019-1882-9

Li, M., Zhang, C., Wang, D., Zhou, L., Wellmann, D., & Tian, Y. (2020). Friction Stir Spot Welding of Aluminium and Copper: A Review. *Materials*, 13(156). https://doi.org/doi:10.3390/ma13010156

Liang, M., Melchers, R., & Chaves, I. (2018). Corrosion and pitting of 6060 series aluminium after 2 years exposure in seawater splash, tidal and immersion zones. *Corrosion Science, 140*, 286–296. https://doi.org/10.1016/j.corsci.2018.05.036

Liao, C., & Wei, R. P. (1999). Galvanic coupling of model alloys to aluminium — a foundation for understanding particle-induced pitting in aluminium alloys. *Electrochimica Acta*, 45(1999), 881–888.

Liz, Z., Li, C., Gao, Z., Liu, Y., Liu, X., Guoa, Q., Yu, L., & Li, H. (2015). Corrosion behaviour of Al–Mg 2 Si alloys with/without addition of Al–P master alloy. *Materials Characterization*, *110(*2015), 170–174, http://dx.doi.org/10.1016/j.matchar.2015.10.028

Lumsden, J. B., Mahoney, M. W., Rhodes, C. G., & Pollock, G. A. (2003). Corrosion Behavior of Friction-Stir-Welded AA7050-T7651. *Corrosion, 59*(3), 212–219. https://doi.org/10.5006/1.3277553

Osório, W. R., Peixoto, L. C., Goulart, P. R., & Garcia, A. (2010). Electrochemical Corrosion Parameters of As-Cast Al-Fe Alloys in a NaCl solution. *Corrosion Science*, 52(2010), 2979–2993, https://doi:10.1016/j.corsci.2010.05.011

Rana, R. S., Purohit, R., & Das, S. (2012). Reviews on the influences of alloying elements on the microstructure and mechanical properties of aluminum alloys and aluminum alloy composites. *International Journal of Scientific and research publications, 2*(6), 1-7.

Rao, A. U., Vasu, V., Govindaraju, M., & Srinadh, K. S. (2016). Stress corrosion cracking behaviour of 7xxx aluminum alloys: A literature review. Transactions of Nonferrous Metals Society of China, 26(6), 1447-1471. https://doi.org/10.1016/S1003-6326(16)64220-6

Rodrigues, E. A. (2012). *Corrosion and mechanical properties tensile and fatigue of aluminum alloy 7050-T73651 in ethanol fuel*. [Thesis Doctoral on Mechanical Engineering], Mechanical Engineering, Faculty of Mechanical Engineering of University of Campinas.

Rosendo, T., Parra, B., Tier, M. A. D., da Silva, A. A. M., dos Santos, J. F., Strohaecker, T. R., & Alcântara, N. G. (2011). Mechanical and microstructural investigation of friction spot welded AA6181-T4 aluminium alloy. *Materials and Design*, 32(2011), 1094–1100, https://10.1016/j.matdes.2010.11.017

Sharma, C., Tripathi, A., Upadhyay, V., Verma, V. & Sharma, S. K. (2021). Friction Stir Spot Welding-Process and Weld Properties: A Review. *Journal of The Institution of Engineers (India): Series D*, 102, 549–565, https://doi.org/10.1007/s40033-021-00276-z

The Welding Institute. (2024). Friction Stir Welding. Available: https://www.twi-global.com/technical-knowledge/job-knowledge/friction-stir-welding-147. Access: 08/02/2024.

Vale, N. L., Torres, E. A., Santos, T. F. A., Urtiga Filho, S. L., & dos Santos, J. F. (2018). Effect of the energy input on the microstructure and mechanical behaviour of AA2024-T351 joint produced by friction stir welding. *Journal of the Brazilian Society of Mechanical Sciences and Engineering*, *40*(467), https://doi.org/10.1007/s40430-018-1372-5

Was, G.S. Ampornrat, P., Gupta, G., Teysseyre, S., West, E. A., Allen, T. R., Sridharan, K., Tan, L., Chen, Y., Ren, X., & Pister, C. (2007). Corrosion and stress corrosion cracking in supercritical water. *Journal of Nuclear Materials*, 371(2007), 176–201, https://doi.org/doi:10.1016/j.jnucmat.2007.05.017

Zeng, F. L., Wei, Z. L., Li, J. F., Li, C. X., Xing, T. A. N., Zhang, Z., & Zheng, Z. Q. (2011). Corrosion mechanism associated with Mg2Si and Si particles in Al–Mg–Si alloys. *Transactions of Nonferrous Metals Society of China*, *21*(12), 2559-2567. https://10.1016/S1003-6326(11)61092-3